ELSEVIER

Colloids and Surfaces
A: Physicochemical and Engineering Aspects 162 (1999) 203–213

COLLOIDS AND SURFACES A

www.elsevier.nl/locate/colsurfa

Stepwise adsorption of a long trichlorosilane and a short aminosilane

Bo Wu, Guangzhao Mao *, K.Y. Simon Ng

Department of Chemical Engineering and Materials Science, Wayne State University, 5050 Anthony Wayne Drive, Detroit, MI 48202, USA

Received 12 February 1999; received in revised form 7 May 1999; accepted 11 May 1999

Abstract

A mixed film of microscopic heterogeneity was formed by stepwise deposition of a long-chain organosilane *n*-octadecyltrichlorosilane (OTS) and a short-chain organosilane aminobutyldimethylmethoxysilane (ABS). The amount of silane deposited on an oxidized silicon substrate was controlled kinetically by varying the dip time in each silane solution. The binary film was characterized by the atomic force microscopy (AFM), infrared attenuated total internal reflection (IR-ATR), and contact angle goniometry. OTS forms a monolayer structure whose fractional surface coverage and surface energy can be precisely controlled. ABS agglomerates slowly to form island structure and is ineffective in surface energy or composition variation. The contact angles on sub-monolayers of OTS follows the Cassie equation, while the contact angle of the binary OTS and ABS film deviates positively from the equation.

Keywords: Chemical adsorption; Mixed films; Self-assembled monolayers; Aggregation; Contact angle hysteresis

1. Introduction

The tremendous advances in the self-assembled monolayers (SAMs) enables one to design model systems with well defined chemical compositions. Heterogeneous surfaces are created by the sub-monolayer deposition, deposition of mixed surfactant monolayers, and the formation of defective spots on a smooth substrate [1]. SAMs of ω-functionalized alkanethiols were shown to incorporate intimately mixed surface groups such as CH_3, CO_2H, OH, CN, CO_2CH_3, and ferrocenyl etc. [2]. But this method requires a metal substrate preferably gold. Many industrial operations involve nonmetallic surfaces such as those of glass fibers and various polymeric materials. These surfaces are often treated with organosilanes. Of all the organosilanes, SAMs of *n*-octadecyltrichlorosilane (OTS) deposited on oxidized silicon substrates from nonpolar organic solvents such as toluene and hexadecane are the best defined system. Experimental studies utilizing a variety of surface characterization methods such as the contact angle goniometry [3], Fourier transform infrared spectroscopy (FTIR) in the specular reflection or the attenuated total internal reflec-

* Corresponding author. Tel.: +1-313-5773804; fax: +1-313-5773810.

E-mail address: gzmao@chem1.eng.wayne.edu (G. Mao)

0927-7757/00/$ - see front matter
PII: S0927-7757(99)00240-X

tion mode (ATR) [4], ellipsometry [5], X-ray photoelectron spectroscopy (XPS) [6], and atomic force microscopy (AFM) [7]. It is generally accepted that OTS follows a Langmuirian irreversible first order adsorption kinetics and forms a closely-packed, chemically linked monolayer structure with a film thickness of 2.6 nm, a film density of 0.21 nm^2 OTS $molecule^{-1}$, and a contact angle of 110° at the adsorption plateau [8].

On the other hand, the surface structure of many other commercial organosilane coatings in particularly those with shorter chains and ω-functionality is poorly understood. Often a monolayer structure is assumed. Aminosilanes with up to 12 carbons in chain length are widely used in polymeric fiber composites as coupling agents and adhesion promoters, immobilization of enzymes, antibodies and colloidal particles, liquid chromatography, and liquid crystal orientation [9]. The surface chemistry and structure of aminosilanes are much less understood and controlled due to a number of factors: the reactivity of the nucleophilic amine with atmospheric CO_2, H_2O, the substrate surface OH group, and the SiOH group of the aminosilane itself [10], and ill-defined 3-D aggregates. Several adsorption mechanisms have been proposed for aminosilanes on oxide surfaces such as the normal adsorption via the silanol group, inverse adsorption via the protonated amino group, and intracyclic form [11]. Multilayer structure of aminosilanes has also been adopted in many interpretations [12]. Moon et al. reported a thin layer formation of 8 Å in thickness in the first 10 min adsorption. Then a multilayer structure was formed by the triethoxy silane, while the films of the monoethoxy and diethoxy silanes remained as monolayers with various amine surface density [13].

In this research, a mixed film was prepared by stepwise deposition of well defined OTS and a less known aminosilane. The mixed film allows one to study the effect of surface heterogeneity on its surface energy. A common surface consists of a continuous phase of one chemical component with randomly dispersed patches of a minor component, often due to contamination, though sometimes formulated to impart additional surface activities. Microscopically heterogeneous films are important in studies of wetting, tribology, microlithography, heterogeneous nucleation and oriented crystal growth. In the case of a multi-component heterogeneous surface, some kind of rules of mixture is generally adopted to predict the overall surface energy, such as the Cassie equation [14]:

$$\cos\theta_C = \chi_1\cos\theta_1 + \chi_2\cos\theta_2, \quad (1)$$

where θ_1, θ_2, and θ_C are the contact angle values of component 1, component 2, and the binary surface, respectively, χ_1 and χ_2 are the fractional surface coverage of component 1 and 2, respectively. Experimentally it is necessary to seek surfaces not only with definable surface roughness and heterogeneity but also resembling wetting surfaces in reality.

In this study, under-deposited as well as binary films formed by a long hydrophobic silane (OTS) and a short hydrophilic silane 4-aminobutyldimethylmethoxysilane (ABS) are characterized by the contact angle goniometry, FTIR-ATR, and AFM. This current system is different from previous studies of co-deposition or stepwise deposition of mixed organosilanes [15] in that it is a microscopically heterogeneous surface instead of a uniformly mixed monolayer formed by both silane species. We want to understand the adsorption and film structure of short organosilane at the microscopic level, the adsorption kinetics of the stepwise surface reaction of a long silane and a short silane, and the effect of hydrophilic micro-domains dispersed in a hydrophobic continuous medium on the overall surface energetics of the binary film.

2. Materials and methods

2.1. Materials

n-Octadecyltrichlorosilane ($C_{18}H_{37}SiCl_3$) or OTS, and 4-aminobutyldimethylmethoxysilane ($NH_2C_4H_9Si(CH_3)_2OCH_3$) or ABS, were purchased from United Chemical Technologies and used as received. Hexadecane (99%) and carbon tetrachloride (99.9%) were purchased from Sigma and used as received. Reagent grade ammonium

hydroxide (NH_4OH), certified 30% hydrogen peroxide (H_2O_2), and reagent grade concentrated nitric acid (HNO_3) were purchased from Fisher Scientific. Water was deionized to 18 MΩ cm resistivity (Nanopure system, Barnstead). Polished N type silicon (111) wafers were purchased from Wafer World Inc. with a thickness of 12–14 mils and resistivity of 50–75 Ω cm. Silicon ATR prisms were single-pass trapezoidal 45° plates, gold coated on one side, with a dimension of $50 \times 10 \times 3$ mm^3, and a total of 17 reflections (Harrick Scientific).

2.2. Organosilane deposition

The silicon substrate was cleaned following the RCA clean procedures used in the integrated circuit manufacturing [16]. The cleaned substrate was used immediately or stored in deionized water. A total of 16 ml hexadecane and 4 ml carbon tetrachloride solution of organosilanes were prepared in a PTFE bottle. The concentration for both OTS and ABS was maintained at 0.007 M while the cumulative dip time of the substrate in each solution was varied. Silane deposition was carried out in the closed PTFE bottle in a N_2-purged glove box. The substrate was sonicated in chloroform for 2 min.

2.3. Characterization

The contact angle was measured by an NRL contact angle goniometer (Model 100, Rame-Hart) in the laboratory atmosphere. A water droplet of 20 μl was placed on the substrate and contact angles were read on both sides of the droplet. Five droplets were placed at various spots near the center of the substrate, and contact angles were averaged with an error of $\pm 3°$.

IR absorption spectra of organosilane films were obtained using a Nicolet Magna-IR 560 single beam spectrometer equipped with a liquid N_2 cooled mercury-cadmium–telluride MCT-A detector, operating at 4 cm^{-1} resolution. A background spectrum of a clean oxidized silicon was recorded before the thin film deposition as a background spectrum. The integrated intensity of the antisymmetric stretching band $\nu(CH_2)$ at 2920 cm^{-1} was used in our study in order to determine adsorbed amount of organosilanes.

AFM images were acquired using Nanoscope IIIa (Digital Instruments) in the contact mode. An e-scanner was used which has a maximum scan size of 16 μm. Only height images were presented here which were captured at highest allowable integral and proportional gains, and a scan rate of 1–5 Hz. Silicon nitride tips were used which have a nominal radius of curvature between 20 and 40 nm and a spring constant of approximately 0.06 N m^{-1}. The width of particulate features cannot be measured accurately due to the tip convolution. Only the height of the microscopic domains was reported here.

3. Results

The stepwise deposition of mixed OTS and ABS films was carried out in two sequences. In Sequence 1, a number of oxidized silicon substrates were dipped in OTS solution for various time periods, and the substrates were then dipped in ABS solution for a fixed time of 1 h. This sequence is denoted as OTS_CABS_{1H}. In Sequence 2, a number of substrates were dipped in ABS solution as a function of time, and then dipped in OTS solution for a fixed time of either 2 s or 10 min. This sequence is denoted as ABS_COTS_{2S} or ABS_COTS_{10M}. Using a short and a long adsorption period of OTS, we hoped to create an ABS dominated surface and an OTS dominated surface. Initially, we also tried the co-deposition of OTS and ABS, but the results were irreproducible. White precipitates were sometimes observed at the bottom of PTFE bottles indicating coagulation between OTS and ABS. Following are the experimental results from the contact angle goniometry, IR-ATR spectroscopy, and AFM measurements.

3.1. Contact angle goniometry

Contact angle data were collected at various time intervals after the first step of deposition, and then on the same substrate after the second step of deposition for a fixed time, thus allowing

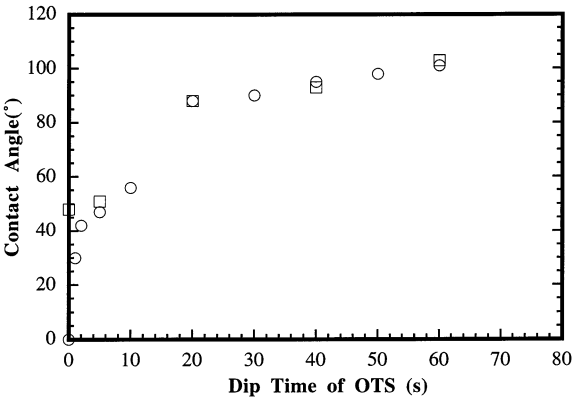

Fig. 1. Plot of the contact angle variation as a function of OTS dip time before (circles) and after (squares) the second step deposition of ABS for a fixed time of 1 h.

the comparison between pure and mixed silanes. Contact angle less than 15° cannot be measured accurately and a 0° was assigned in such cases. The contact angle was plotted against the cumulative dip time of OTS in Fig. 1 for OTS_CABS_{1H}, and of ABS in Fig. 2 for ABS_COTS_{2S} and ABS_COTS_{10M}.

In Fig. 1, the contact angle rose monotonically and reached a plateau at 110° after approximately 1 min of OTS adsorption. The plateau value indicates a surface covered by terminal methyl groups. The adsorption curve of OTS agrees well with literature values obtained under similar conditions [17]. The smooth rise of contact angles

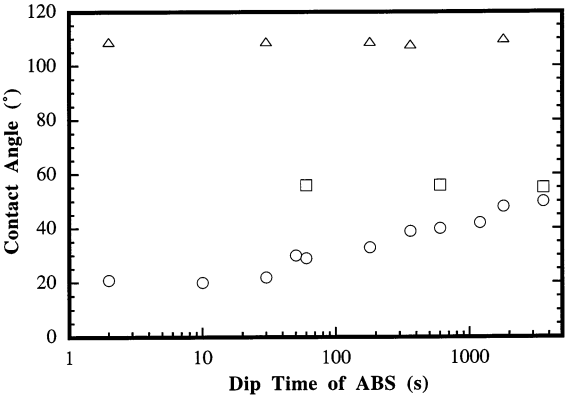

Fig. 2. Plot of the contact angle variation as a function of ABS dip time before (circles) and after 2 s (squares) or 10 min (triangles) dipping in OTS solutions.

within 1 min of OTS adsorption implies that the surface energy of oxidized silicon can be controlled in the full range from extremely hydrophilic (0°) to extremely hydrophobic (110°) simply by varying the cumulative dip time of OTS alone. The contact angle increase can be made more gradual by lowering the concentration of OTS [26]. Except on surfaces with only very low OTS coverage (or a few seconds dip time), ABS had no influence on the overall contact angles as shown in Fig. 1. A total of 1 h deposition of ABS alone renders the substrate more hydrophobic with a measurable contact angle of 48°. Adsorption of ABS onto fully covered OTS is not possible due to the lack of reactive sites. The data show that the presence of OTS even a small amount, either prevents the adsorption of ABS, or somehow is more dominating in the overall contact angle.

Fig. 2 shows the contact angle variation in Sequence 2 where ABS was deposited in the first step as a function of time and OTS in the second step with a fixed time. The adsorption of ABS is sluggish. The contact angle increased gradually from 0 to 40° within 600 s of dip time. The maximum contact angle measured during 24 h of immersion was approximately 50°. The value is close to and perhaps a little less than some of the contact angles measured on similar aminosilane surfaces. For example, a 54° was measured on aminopropyltriethoxysilane (APS) [18] and lysine terminated surfaces [19]. Others have measured the contact angle of 100% amine termination to be 63° while ammonium termination to be 42° [20]. The slow adsorption kinetics suggests a gradual surface aggregation, polymerization, or multilayer formation. Both surface reaction and agglomeration can occur simultaneously for organosilanes containing nucleophilic groups such as amine [21]. Due to various reaction mechanisms, the surface after aminosilane deposition may have a variety of surface groups such as amine, ammonium, ammonium bicarbonate, methylene, methyl, and silanol. Therefore agglomeration of ABS significantly reduces the surface density of the amine group. In the second step, two fixed periods were used. A total of 2 s OTS deposition produced a contact angle of 42°, and

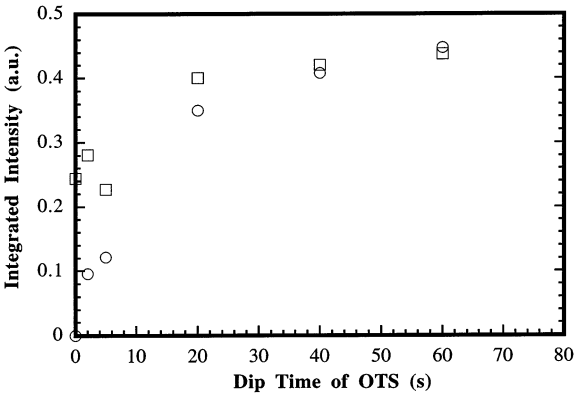

Fig. 3. Plot of the integrated intensity of $\nu(CH_2)$ antisymmetric stretching band variation as a function of OTS dip time before (circles) and after 1 h (squares) dipping in ABS solutions.

10 min OTS deposition yielded a contact angle of 110°. In Fig. 2, contact angles for the mixed film display the two horizontal lines one maintained at 55° for 2 s OTS deposition and one at 110° for 10 min OTS deposition. The constant values again indicated the ineffectiveness of the ABS component in the variation of the binary film surface energy. Is this ineffectiveness a result of low adsorbed amount of ABS or something much more complicated in nature? In order to answer this question, we also carry out IR-ATR and AFM study on the same surfaces.

We also want to point out that the solubility of ABS in water is not an issue in contact angle measurement. All the organic soluble ABS was presumably removed by rinsing the ABS covered surface with copious amount of chloroform. An IR experiment was conducted where the integrated intensity of the $\nu(CH_2)$ *anti*-symmetric stretching band was measured before and after leaving the ABS covered sample (1 h dip time in ABS solution) in water for 10 min. The contact angle measurement on the other hand takes only a few minutes to complete. No reduction in the integrated intensity of the band was observed.

3.2. IR-ATR spectroscopy.

Figs. 3 and 4 are plots of the relative integrated intensity of $\nu(CH_2)$ antisymmetric stretching band, at approximately 2920 cm^{-1} versus the dip time after the first step and after the second step deposition for Sequence 1 and 2, respectively. Only the CH_2 band was used to follow the surface coverage of both OTS and ABS because the NH_2 and NH_3^+ bands were too weak to be detected.

Fig. 3 shows the same initial rapid increase in surface coverage until the plateau was reached at approximately 1 min of OTS deposition, agreeing well with the kinetic study by the contact angle measurement (Fig. 1). Both measurements indicated a Langmuirian irreversible first order kinetics. The relative peak intensity of OTS is comparable to the literature values of similar systems indicating a monolayer coverage instead of 3-D agglomeration. A maximum integrated intensity of 0.456 was maintained after 30 min of deposition. An additional dipping in ABS solution for 1 h resulted in a significant increase in the intensity only when the same surface was kept in OTS solution for no more than 40 s. After 20 s OTS adsorption, the surface coverage is increased to 75%, ABS adsorption was still observed. Some have reported that half a monolayer of randomly distributed OTS molecules reduced the reactive area of oxidized silicon to 5% [22]. Our results show that it takes 90% OTS coverage to effectively inhibit the ABS deposition, while it takes only 30% OTS coverage for it to dominate the contact angle measurement.

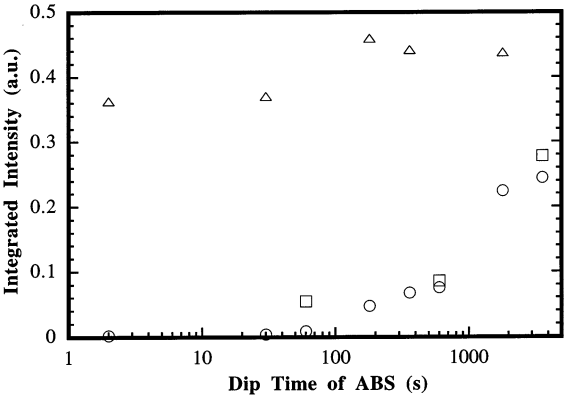

Fig. 4. Plot of the integrated intensity of $\nu(CH_2)$ antisymmetric stretching band variation as a function of ABS dipping time before (circles) and after 2 s (squares) or 10 min (triangles) dipping in OTS solutions.

Fig. 4 shows a monotonic yet sluggish increase in the adsorbed amount in the first hour of ABS adsorption. Significant increase in the adsorbed amount occurred after 100 s until 24 h which was the longest time interval used in our study. On the contrary, the contact angle change was more gradual throughout the dipping and reached a plateau at around 600 s. Only 2 s of OTS adsorption resulted in a slight yet measurable increase in the integrated intensity due to the extremely short dip time of OTS. On the other hand, the integrated intensity increased significantly when the dip time in OTS was increased to 10 min. In the absence of ABS, the coverage of OTS after 10 min is approximately 100%. After 2 min ABS adsorption, OTS can reach 90% monolayer coverage, after 30 min of ABS adsorption, the ultimate OTS surface coverage was lowered to 50% but still significant. This strongly indicated that the surface coverage of ABS at best reached 50%, probably as a result of weak ABS and substrate interaction. Our results agree with literature values [13]. It is thus unlikely that OTS deposits on top of ABS layer or exchanges with ABS. It is interesting to notice that for a surface with equal surface coverage of OTS and ABS, the contact angle 110° reflects a surface of pure methyl termination. The contact angle phenomenon of a mixed film described above is apparently very complicated and does not follow a simple rule of mixture.

3.3. Atomic force microscopy (AFM)

In order to quantify the film roughness and aggregate size we carried out AFM study on films prepared at various deposition intervals and stages. Selective AFM results are shown in Fig. 5a–d and the complete surface analysis of roughness and particle height results are summarized in Table 1.

The surfaces of a clean oxidized silicon with 0, 25, and 100% OTS coverage (Fig. 5a) are molecularly smooth. No aggregates can be detected on OTS films of various coverage indicating a uniform monolayer assembly. No molecular lattice structure was captured on OTS films due to the amorphous nature of the underlying oxidized silicon. Fig. 5b is the surface after dipping in ABS solutions for 1 h showing individual particles randomly distributed. After 30 s of ABS adsorption, no particles were found on the surface suggesting a sparse monolayer formation in the early stage. The average particle size increased from 1.4 to 6.5 nm with increasing dip time up to 24 h. AFM images provide the definitive proof of a multilayer buildup or 3-D agglomeration of ABS, most likely due to physisorption, which proceeds very slowly in contrast to the fast adsorption kinetics of monolayers.

The films after the second step immersion were also examined by AFM. After 5 s OTS adsorption, the surface coverage was about 25%, 3-D islands of ABS with an average height of 5.2 nm are shown in Fig. 5c, not much different from that of ABS in the absence of OTS in Fig. 5b. When the surface was fully covered by OTS, the surface aggregation of ABS was inhibited. No surface topographical changes were observed when first step is the ABS adsorption and the second step is the OTS deposition of a fixed 2 s or 10 min (Fig. 5d). This implies that ABS domains coexisted with the sub-monolayers of OTS. Our results have shown that OTS forms a 2-D structure on oxidized silicon surface, while ABS forms at least a partial 3-D structure on the same surface.

4. Discussion

In order to understand the adsorption kinetics and wetting properties of a mixed film, it is necessary to compute the fractional surface coverage of each component. The computation of OTS fractional coverage is straightforward because the data from contact angle, AFM, and IR-ATR all point to a monolayer structure. The fractional surface coverage of OTS, χ_{OTS}, is estimated using the corresponding CH_2 integrated IR intensity, I_{OTS}:

$$\chi_{OTS} = \frac{I_{OTS}}{I_{100\%}}, \quad (2)$$

where the relative integrated intensity at the adsorption plateau, 0.456, was taken as that of a

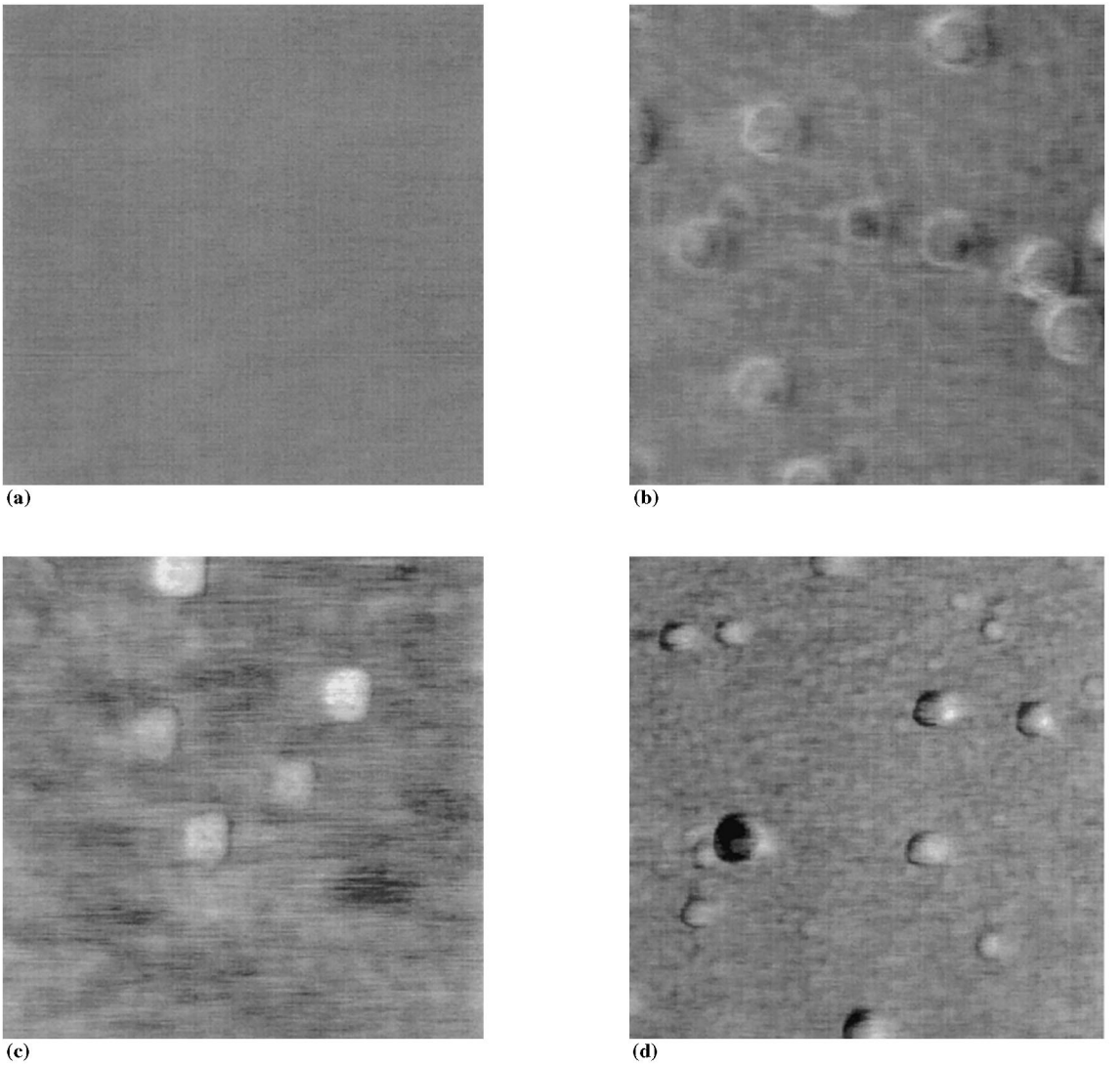

Fig. 5. AFM height images of oxidized silicon substrate surfaces at a constant force, captured in ambient environment: (a) after 30 min dipping in OTS solution; (b) after 1 h dipping in ABS solution; (c) after 5 s in OTS and 1 h in ABS; and (d) after 1 h in ABS and 10 min in OTS. The scan size is 1×1 μm^2.

fully covered OTS film $I_{100\%}$. The validity of the Cassie equation is verified using the partial monolayer of OTS on oxidized silica surface. Fig. 6 displays the measured contact angles and the theoretical values (θ_C) versus the fractional surface coverage of OTS (χ_{OTS}). The theoretical contact angle is calculated using χ_{OTS} based the IR data and the Cassie equation [23]:

$$\cos\theta_C = 1 - 1.34 \times \frac{I_{OTS}}{I_{100\%}}. \quad (3)$$

The contact angles of water on pure SiO_2 and OTS are 0 and 110°, respectively. Our data, though limited in numbers, agree fairly well with those from the above calculations (Fig. 6). This monotonic increase in the contact angle with the adsorbed amount of OTS allows a precise control of the oxidized silicon surface energy.

Table 1
AFM measurements of the mean surface roughness R_a and the average particle height

Type of surfaces	Surface roughness R_a (nm)	Particle height (nm)
SiO_2	0.21	No particle
OTS_{5S}	0.29	No particle
OTS_{30M}	0.07	No particle
ABS_{30S}	0.08	No particle
ABS_{1M}	0.24	1.45
ABS_{1H}	1.69	5.40
ABS_{24H}	1.10	6.50
$OTS_{5S}ABS_{1H}$	1.30	5.20
$OTS_{30M}ABS_{1H}$	0.54	No particle
$ABS_{30S}OTS_{10M}$	0.67	No particle
$ABS_{1M}OTS_{2S}$	1.75	1.20
$ABS_{1H}OTS_{10M}$	0.89	6.20
$ABS_{24H}OTS_{2S}$	1.20	6.80

Attempts to verify the Cassie equation against the adsorption of ABS on oxidized silicon prove to be difficult due to the multilayer buildup and uncertainty in the surface functionality of ABS domains. Firstly, the adsorption does not follow the Langmuirian kinetics. From our data, a most likely mechanism of ABS deposition is the simultaneous formation of ABS monolayer with low surface coverage, and the slow development of a multilayer structure. As a result, the fractional surface coverage of ABS is unknown. Secondly, the exact contact angle of a fully covered ABS monolayer cannot be extracted accurately from the contact angle measurement. In order to gain some insights into mechanism of the ABS adsorption and its effect on the surface energy, the integrated IR intensity data is normalized by the theoretical value of a fully covered monolayer of ABS. For simplicity, we assume ABS exhibiting the same IR absorbance per CH_2 as derived from OTS, a neat liquid density of 0.777 g cm^{-3} for the hydrolyzed ABS domain, a density of 0.954 g cm^{-3} for the cross-linked, closely-packed OTS domain, a monolayer thickness 0.8 nm based on the ABS molecular chain length, and a height of 2.6 nm for a monolayer of OTS [18]. The fractional surface coverage of ABS monolayer, χ_{ABS}, is then calculated using the following conversion factor [24]:

$$\chi_{ABS} = 8.0 \times \frac{I_{ABS}}{I_{100\%}}. \quad (4)$$

According to the above equation, 100% ABS monolayer coverage will give a relative integrated IR intensity of 0.057. The apparent average number of ABS layers is computed as $I_{ABS}/0.057$, and is plotted against the dip time in Fig. 7a. It shows a very slow buildup of layers. An adsorbed amount equivalent to a monolayer coverage is reached at 200 s, double layer at 800 s, and five layer at 8000 s. The average layer thickness based on the simplified model is within the limits set by the AFM measurement.

Now we apply the same methodology to the stepwise adsorption of OTS and ABS, and plot the net number of layers of OTS and ABS as a function of dip time for Sequence 1 and 2 in Fig. 7b and c, respectively. As OTS approaches 100% monolayer coverage, the coverage of ABS diminishes as expected. But the amount of ABS is much higher than what is necessary to backfill the submonolayer of OTS due to the multilayer structure. Even when available surface area is reduced to 20%, ABS can adsorb to an amount equivalent to that of a monolayer. In the absence of OTS, the ABS layer thickness after 1 h dip time can reach 4.2 nm on an average according to IR, and 5.4 nm for the highest domains according to AFM. But with the significant amount of ABS present in

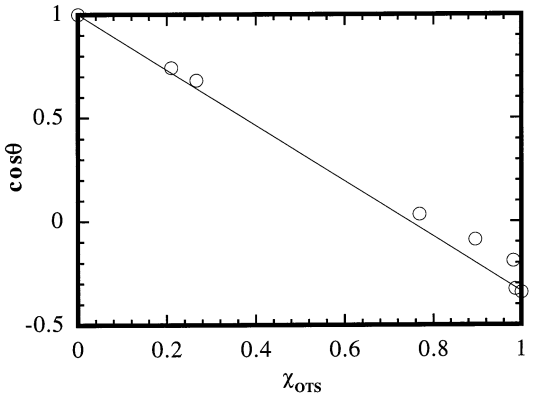

Fig. 6. Plot of the cosine of the contact angle versus the fractional surface coverage of OTS. The circles represent experimental contact angle values and the line is the Cassie equation.

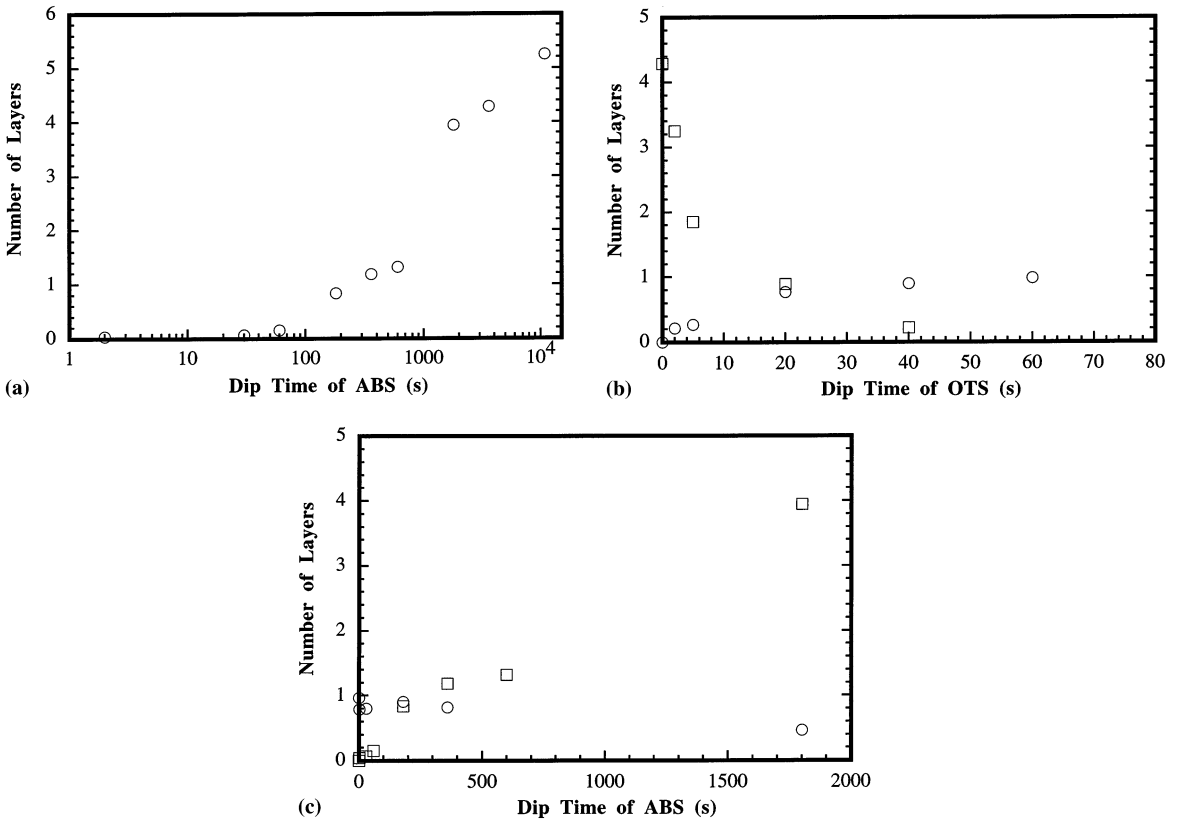

Fig. 7. (a) Plot of the apparent number of ABS monolayers as a function of ABS dip time; (b) plot of the OTS fractional surface coverage (circles) and the apparent number of ABS monolayers (squares) as a function of OTS dip time for Sequence OTS_CABS_{1H}; (c) plot of the OTS fractional surface coverage (circles) and the apparent number of ABS monolayers (squares) as a function of ABS dip time for Sequence ABS_COTS_{10M}.

the mixed film, its surface energy as measured by the contact angle goniometry is almost totally dependent on the OTS domains, while the ABS domains behave like the oxidized silicon surface. Due to the lack of information on the surface coverage of ABS in Sequence 1, we cannot compare the experimental results with the Cassie equation. In Sequence ABS_CABS_{10M} as shown in Fig. 7c, as the adsorbed amount of ABS increases, the amount of OTS allowed on the surface decreases as expected. But the ABS layer at most reduces the amount of OTS by half which also implies a highly discontinuous film of ABS. There is a possibility of OTS reacting directly on top of the OTS film, but the fact that the surface coverage of OTS is reduced in the presence of ABS does not favor this mechanism. The exchange of ABS by OTS is also not likely since the removal of the physically adsorbed ABS during chloroform rinsing. It is intriguing that the contact angle of the mixed film with 50% OTS surface coverage was 110°. According to the Cassie equation, the contact angle of 50% OTS and 50% NH_2 terminated ABS surface should be 87°, while the contact angle of 50% OTS on oxidized silicon is 71°. A reason for the positive deviation is the pinning of an advancing droplet on a more hydrophobic patch which exaggerates the contribution from the hydrophobic fractional surface area [25]. Surface roughness can also exaggerate the contribution from the hydrophobic domain. More accurate information concerning the deviation from Cassie equation can be obtained from the contact angle hysteresis measurement using dynamic contact an-

gle techniques on such surfaces. Drelich et al. correlated the surface aggregate structure of unsaturated carboxylic acids on a fluorite surface with the contact angle hysteresis, and found a maximum hysteresis occurring at a submonolayer adsorption density between 3 and 5 μmol m^{-2} [26].

5. Conclusions

The stepwise adsorption of a long trichlorosilane (OTS) and a short aminosilane (ABS) on the oxidized silicon wafer surface was studied by the contact angle goniometry, infrared attenuated total internal reflection (IR-ATR), and atomic force microscopy (AFM). OTS forms a smooth monolayer which follows Langmuirian irreversible first order kinetics, while ABS forms three-dimensional multilayer domains of up to 7.0 nm in thickness. The adsorption of ABS is very sluggish. The OTS sub-monolayer on oxidized silicon surface follows the Cassie equation. But the binary film of OTS and ABS deviates positively from the Cassie prediction. The deviation may be due to the surface roughness and chemical heterogeneity at the nanometer to sub-micrometer scale. Practically, the well defined surface adsorption of OTS enables one to gradually vary the surface energy from an extremely hydrophilic to extremely hydrophobic. On the other hand, aminosilane coating for biosensors and fiber/matrix coupling does not have simple surface physical and chemical structure as often assumed. The fractional surface coverage of amine functional groups can be much less than anticipated. Mixed OTS and ABS films are not an effective system for surface energy or even surface functionality variation. But they can potentially be used to study the effect of microscopic surface heterogeneity and roughness on the surface energetics. It will be interesting to measure the contact angle hysteresis using dynamic contact angle techniques on such surfaces.

Acknowledgements

The Graduate Research Assistantship program of the Institute for Manufacturing Research at Wayne State University (WSU) is acknowledged for the support of this research. Professor Mao acknowledges partial support from the Career Program of the National Science Foundation CTS-9703102, the Donors of the Petroleum Research Fund no. 31280-G7, administered by the American Chemical Society. Professor Ng acknowledges the Donors of the Petroleum Research Fund no. 33036-AC, administered by the American Chemical Society.

References

[1] (a) P.E. Laibinis, M.A. Fox, J.P. Folkers, G.M. Whitesides, Langmuir 7 (1991) 156. (b) S.D. Evans, R. Sharma, A. Ulman, Langmuir 7 (1991) 3167. (c) C. Andrieu, C. Sykes, F. Brochard, Langmuir 10 (1994) 2077. (d) J.-M. di Meglio, Europhys. Lett. 17 (1992) 607.

[2] (a) A. Ulman, An Introduction to Ultra Thin Organic Films from Langmuir-Blodgett to Self-Assembly, Academic, Boston, 1991. (b) C.D. Bain, J. Evall, G.M. Whitesides, J. Am. Chem. Soc. 111 (1989) 7155. (c) L.H. Dubois, R.G. Nuzzo, Annu. Rev. Phys. Chem. 43 (1992) 437. (d) A. Ulman, S.D. Evans, Y. Shnidman, R. Sharma, J.E. Eilers, Adv. Colloid Interf. Sci. 39 (1992) 175.

[3] S.R. Wasserman, Y.-T. Tao, G.M. Whitesides, Langmuir 5 (1989) 1074.

[4] (a) R. Maoz, J. Sagiv, J. Colloid Interf. Sci. 100 (1984) 465. (b) A. Ulman, J.S. Schildkraut, T. Penner, J. Am. Chem. Soc. 110 (1988) 6136. (c) D.L. Angst, G.W. Simmons, Langmuir 7 (1991) 2236. (d) C.P. Tripp, M.L. Hair, Langmuir 8 (1992) 1120. (e) K. Mathauer, C.W. Frank, Langmuir 9 (1993) 3446. (f) R. Banga, J. Yarwood, A.M. Morgan, Langmuir 11 (1995) 618.

[5] (a) M.E. McGovern, K.M.R. Kallury, M. Thompson, Langmuir 10 (1994) 3607. (b) I.M. Tidswell, T.A. Rabadeau, P.S. Pershan, S.D. Kosowsky, J. Chem. Phys. 95 (1991) 2854. (c) M. Wei, R.S. Bowman, J.L. Wilson, N.R. Morrow, J. Colloid Interf. Sci. 157 (1993) 154.

[6] E. Frydman, H. Cohen, R. Maoz, J. Sagiv, Langmuir 13 (1997) 5089.

[7] (a) D.K. Schwartz, S. Steinberg, J. Israelachvili, J.A.N. Zasadzinski, Phys. Rev. Lett. 69 (1992) 3354. (b) S. Peach, R.D. Polak, C. Franck, Langmuir 12 (1996) 6053.

[8] (a) P. Guyot-Sionnest, R. Superfine, J.H. Hunt, Y.R. Shen, Chem. Phys. Lett. 144 (1998) 1. (b) S.S. Cheng, D.A. Scherson, C.N. Sukenik, J. Am. Chem. Soc. 114 (1992) 5436. (c) A. Ulman, J.S. Schildkraut, T.L. Penner, J. Am. Chem. Soc. 110 (1988) 6136.

[9] E.P. Plueddemann, Silane Coupling Agents, 2nd, Plenum, New York, 1991.

[10] (a) K. Bierbaum, M. Kinzler, Ch. Wöll, M. Grunze, G. Hähne, S. Heid, F. Effenberger, Langmuir 11 (1995) 512. (b) D.G. Kurth, T. Bein, Angew. Chem. Int. Ed. Engl. 31 (1992) 336. (c) K.M.R Kallury, P.M. MacDonald, M. Thompson, Langmuir 10 (1994) 492.
[11] K.L. Mittal (Ed.), Silanes and Other Coupling Agents, VSP, The Netherlands, 1992.
[12] T.W. Wang, F.D. Blum, J. Mater. Sci. 31 (1996) 5231.
[13] (a) J.H. Moon, J.W. Shin, S.Y. Kim, J.W. Park, Langmuir 12 (1996) 4621. (b) J.H. Moon, J.H. Kim, K.-J. Kim, T.-H. Kang, B. Kim, C.-H. Kim, J.H. Hahn, J.W. Park, Langmuir 13 (1997) 4305.
[14] A.B.D. Cassie, Discuss. Faraday Soc. 3 (1948) 11.
[15] (a) J. Sagiv, J. Am. Chem. Soc. 102 (1980) 92. (b) P. Harder, K. Bierbaum, Ch. Woell, M. Grunze, S. Heid, F. Effenberger, Langmuir 13 (1997) 445. (c) K. Mathauer, C.W. Frank, Langmuir 9 (1993) 3002.
[16] W. Kern, J. Electrochem. Soc. 137 (1990) 1887.
[17] D.H. Flinn, D.A. Guzonas, R.-H. Yoon, Colloids Surf. A 87 (1994) 163.
[18] D. Kowalczyk, S. Slomkowski, M.M. Chehimi, M. Delamar, Int. J. Adhes. Adhes. 16 (1996) 227.
[19] K.A. Woodhouse, J. Brash, J. Colloid Interf. Sci. 154 (1992) 327.
[20] N. Balachander, C.N. Sukenik, Langmuir 6 (1990) 1621.
[21] C.P. Tripp, M.L. Hair, J. Phys. Chem. 97 (1993) 5693.
[22] D.L. Allara, A.N. Parikh, E. Judge, J. Chem. Phys. 100 (1994) 1761.
[23] $\cos\theta_C = \cos\theta_{SiO_2}\chi_{SiO_2} + \cos\theta_{OTS}\chi_{OTS}$
$= \cos\theta_{SiO_2}(1-\chi_{OTS}) + \cos\theta_{OTS}\chi_{OTS}$
$= 1 - 1.34 \times \frac{I_{OTS}}{I_{100\%}}$
[24] $\frac{\chi_{ABS}}{\chi_{OTS}} = \frac{I_{ABS}}{I_{OTS}} \times \frac{M_{ABS}}{M_{OTS}} \times \frac{n_{OTS}}{n_{ABS}} \times \frac{\rho_{OTS}}{\rho_{ABS}} \times \frac{H_{OTS}}{H_{ABS}} = 8.00\frac{I_{ABS}}{I_{OTS}}$,
where M, n, ρ, and H are the molecular weight, number of CH_2 per molecule, density, and monolayer thickness of ABS and OTS, respectively.
[25] J. Drelich, Pol. J. Chem. 71 (1997) 525.
[26] J. Drelich, J.A.A. Atia, M.R. Yalamanchili, J.D. Miller, J. Colloid Interf. Sci. 178 (1996) 720.